Soudi, S. & Rahman, B. M. (2014). Design of compact polarization rotator using simple silicon nanowires. Applied Optics, 53(34), pp. 8071-8077. doi: 10.1364/AO.53.008071

Design of Compact Polarization Rotator using simple Silicon nanowires

S. Soudi, B. M. A. Rahman,*

School of Engineering and Mathematical Sciences, Northampton Square, London EC1V OHB, UK
*Corresponding author: B.M.A.Rahman@city.ac.uk

Received Month X, XXXX; revised Month X, XXXX; accepted Month X, XXXX;
posted Month X, XXXX (Doc. ID XXXXX); published Month X, XXXX

In this paper, an ultra-compact design of polarization rotator based on silicon-on-insulator platform is presented, which contains two simple silicon nanowires but with unequal in width, which will be easier to fabricate. It is shown here that a low-loss, wide bandwidth and 52.8 μm long compact Polarization rotator with polarization cross-talk -20 dB can be achieved. A full-vectorial finite element method and the least squares boundary residual method are used to study the effects of the fabrication tolerances and this design shows reasonably stable performances.

OCIS codes: (000.4430) Numerical approximation and analysis; (999.9999) Finite element method; (130.5440) Polarization-selective devices; (350.4238) Nanophotonics crystals; (040.6040) Silicon; (260.5430) Polarization; (250.5300) Photonic integrated circuits; (130.3120) Integrated optics devices.

1. Introduction

Revolution of the electronic technology was only possible due to both miniaturization and integration of millions of transistors into a single VLSI chip. On the other hand, unlike highly developed, low-cost, user friendly electronic goods, optical communication systems of today rely heavily on hybrid integration of a limited number of relatively larger discrete components like lasers, modulators, multiplexers, detectors etc. Similar to the revolution that single chip integration brought to electronics, one way to reduce the cost of optoelectronics, is to make the devices as small as possible and find a material system for monolithic integration of all the components.

Photonic Integrated Circuit (PIC) can improve reliability and reduce the size of a complex device by using fewer components. However, so far there has not been a large-scale PIC commercially deployed because of the high development cost and poor flexibility associated with the fabrication processes of the monolithically integrated subsystems. One way of reducing the device size is to use a dielectric material with a refractive index as high as possible, which can improve the optical confinement and effectively reduce the waveguide dimensions. High index contrast also allows very small bending radius, suitable for increasing number of components on a chip to increase both functionality and reliability of the chip.

Silicon (Si) is the most mature material for electronics but relatively a newer material for photonics. The expensive compound semiconductor materials, such as GaAs or InP can provide light sources, but their low yield coupled with the higher assembly and packaging costs, keep optical communication a costly technology today. Recently, it has been suggested [1] that silicon with silicon-on-insulator technology (SOI) can be considered to be a material choice for designing and integrating dense PIC and optoelectronic integrated circuit (OEIC) devices.

As the telecommunication industry embraces for a higher optical transmission network, the importance of minimizing the unexpected polarization rotation and polarization crosstalk to compensate the polarization mode dispersion (PMD) in the optical transmission network is of great interest. It is well known that modes in optical waveguides with two-dimensional confinement are hybrid in nature, with all the 6 components of their **E** and **H**-fields being present. Circularly symmetric optical fiber cannot maintain its polarization state as signal travels through bends, stressed sections or some small irregularities. As a result, light input to an integrated optical chip can be randomly polarized. This polarization of light has a great impact on both photonic circuit design and operation. Therefore it is desirable to have a fixed degree of polarization state, such as transverse electric (TE) or transverse magnetic (TM) polarization state and it may be necessary to rotate an incoming polarization state by incorporating polarization splitter and polarization rotator (PR).

It was reported that polarization rotation can be achieved by exploiting the electro-optic effect in $LiNbO_3$ [2] and InP [3]. However it was also suggested that passive polarization converter [4] would be preferable because it would be much simpler to fabricate and to process. Earlier passive polarization converter based on the use of asymmetrically periodic loaded [5] or cascaded [6] waveguides have also been reported, but such converter has a relatively large device length. To minimize the device length and to reduce the excess loss, a single-section

passive polarization rotator [7] has been suggested, but it may require a complicated fabrication process often due to its tilting [8] or slanting sidewalls [9, 10], or with an asymmetric notch [11].

Recently, PR made of horizontal slot and strip waveguide (WG) has been reported based on mode evolution [12]. Its fabrication is not easy as the required control of tapered structure is relatively difficult to realize. Moreover, it can rotate only one polarization state for one input direction. Simpler PR by using vertical slots guides have also been reported [13, 14, 15]. Three WGs-based polarization splitter and rotator have also been reported [16]. Another approach is made for this TE-TM conversion based on 2-D photonic crystal slab WG [17]. In this case, though the conversion has been good, but the structure itself is complicated. Researchers have also tried to implement TE to TM convertor by increasing the polarization crosstalk in μ-bend Si WG [18] or bent guide with slanted side wall [19]. Here the conversion efficiency is high though very sensitive to issues like bend loss, slant angle, smooth wall of the WG around bent region etc.

The Si polarization rotator proposed here shows a very compact design without slanted side wall or bent. In this paper, design optimization of a Si polarization rotator based on SOI technology is presented which requires less complex fabrication process with single mask only and compatible with the mature CMOS technology which is backed by a well-established semiconductor industry. The conversion of one polarized mode to the orthogonal polarized mode is realized by efficient power coupling between these two polarized modes at the *phase matching* or *resonance* condition. The Si polarization rotator reported here has a relatively small footprint and has very low loss compared with the other polarization rotator so far reported.

2.Theory

Pure TE and TM modes can only exist in planar slab waveguides with 1-dimensional confinement. However, in all practical optical waveguides with 2-dimensional confinement, the modes are classified as quasi-TE and quasi-TM modes, which contain all the 6 components of the **E** and **H** fields. Besides that, in the high index contrast silicon nanowires, the modal hybridness is much higher. To find all the 3 components of the **H**-field and the evolution of fully hybrid quasi-TE and quasi-TM modes along a guided-wave device all the methods to be used must be fully vectorial in nature.

Accurate calculation of the magnitudes of the non-dominant field components and their profiles for the fundamental quasi-TE and quasi-TM polarized modes are of great importance when designing a polarization rotator. In the design of a compact optical polarization rotator, a full vectorial finite element method (VFEM) is needed and used here to obtain the modal field profiles of the constituent waveguides. In this formulation all the **H**-field components are continuous across the dielectric interface. On the other hand since normal component of the **E**-field is discontinuous around the interface, an equivalent **E**-field based approach would be less satisfactory. As for the hybrid modes, a significant non-dominant field component exist around the dielectric interfaces, hence, **H**-field formulation can treat such waveguides more rigorously. In the design process, it is necessary not only to increase the magnitude of the non-dominant field components but also its profile can also be optimized to enhance its overlap with the dominant field components to achieve maximum polarization rotation. The full-vectorial formulation used here, is based on the minimization of the following energy functional [20] in terms of the nodal values of the full **H**-field vector:

$$\omega^2 = \frac{\int\left[(\nabla \mathbf{x}\mathbf{H})^*.\varepsilon^{-1}(\nabla \mathbf{x}\mathbf{H})+p(\nabla.\mathbf{H})^*(\nabla.\mathbf{H})\right]dxdy}{\int \mathbf{H}^*.\mu\mathbf{H}dxdy} \quad (1)$$

where **H** is the full vectorial magnetic field, * denotes a complex conjugate and transpose, ω^2 is the eigenvalue where ω is the angular frequency of the wave and ε and μ are the permittivity and permeability, respectively. The penalty function approach has also been incorporated to impose divergence-free condition of the magnetic field to reduce the appearance of spurious modes and p is the dimensionless penalty parameter. This full-vectorial FEM modal solution is also used to determine the polarization beat length between the two quasi-TE and quasi-TM polarized fundamental modes.

A beam propagation method (BPM), which must be fully vectorial [21], can be used to calculate the power conversion between the two polarization states. On the other hand, a junction analysis approach can also be used, as the proposed polarization rotator structure is composed of only two butt-coupled uniform waveguide sections with only two discrete interfaces between them. A powerful numerical approach, the Least Squares Boundary Residual (LSBR) method [22] can also be used, which rigorously satisfies the continuity of the tangential electric and magnetic fields at the junction interface in a least squares sense, and obtains the modal coefficients of the transmitted and reflected fully hybrid modes at the discontinuity interface. The LSBR method looks for a stationary solution to satisfy the continuity conditions by minimizing the error energy functional, J, as given by [22]

$$J = \int_\Omega |E_t^I - E_t^{II}|^2 + \alpha.Z_0^2|H_t^I - H_t^{II}|^2 d\Omega \quad (2)$$

where Z_0 is the free-space impedance and α is the dimensionless weighting factor to balance the electric and magnetic components of the error functional J. The integration is carried out at the junction interface, Ω, between the straight and the asymmetric Si waveguides. This approach would be more rigorous and computationally more efficient than the use of the BPM for this structure.

3. Results

The schematic cross-section of the polarization rotator is shown which consist of two silicon nanowires (NW) but with unequal width. They are of equal height, identified by *H* which would be easy to fabricate. However, they have different widths, given here as W_{TE} and W_{TM}, to achieve phase matching between the quasi-TE (H^{y}_{11}) and quasi-TM (H^{x}_{11}) polarized modes of these two waveguides with unequal widths. The separation between the guides is *S*, as shown here. The refractive index of the silicon and silica are taken as 3.4754752 and 1.4440236 at the operating wavelength of 1.55 μm.

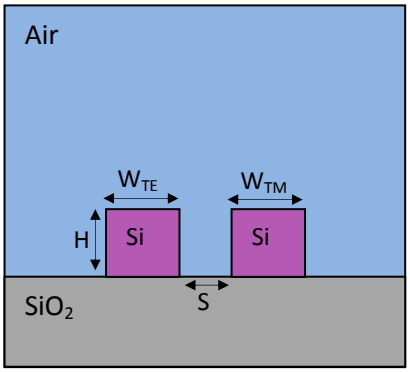

Fig. 1. Schematic diagram of a polarization rotator.

It is well known that propagation constants or the effective indices of the two polarized modes are different for a high index contrast Si NW due to structural non-symmetry. Variations of the effective indices, n_{eff} of the quasi-TE (H^{y}_{11}) and quasi-TM (H^{x}_{11}) modes for *isolated* silicon NW waveguide with height, H = 260 nm and 300 nm are shown in Fig.2. It can be observed that when the width of the guide is large the effective indices reach that of a slab waveguide (with the same height) asymptotically. However, as the width is reduced, initially effective indices reduce slowly and then quite rapidly as the cutoff width is approached. It can be noticed that effective indices of the H^{y}_{11} mode is higher than that of the H^{x}_{11} mode, particularly when the width is large. It can be noted, but not clearly obsorved that H^{x}_{11} mode approaches its cutoff when the width is lower than 200 nm and 150 nm, for H = 260 nm and 300 nm, respectively. Similarly the H^{y}_{11} modes approach their cutoff when W is reduced below 265 nm and 260 nm for H = 260 nm and 300 nm, respectively.

Since for most of the Si NW the effective indices of the H^{y}_{11} and H^{x}_{11} modes are not equal, so a directional coupler using two identical NWs, the H^{y}_{11} mode in one guide will not be phase matched to H^{x}_{11} mode in the other guide. However, by using unequal widths for these two guides H^{y}_{11} mode in one guide can be phase matched to the H^{x}_{11} mode in the other guide. Next, we have studied the necessary width of a guide (W_{TE}) supporting the H^{y}_{11} mode to be phase matched with another guide with width (W_{TM}) supporting the H^{x}_{11} mode. Variations of the W_{TE} necessary to phase match a guide with quasi-TM mode are shown in Fig.3 for 3 different waveguide heights, *H*. As example, for the height 260 nm, shown by a red dashed line, and when the width of W_{TM} is 600 nm, the width necessary (W_{TE}) for phase matching its quasi-TE mode is 353 nm and at this time effective indices for both the modes are 2.00. However, this phase matching condition shown here is strictly valid only for the isolated guides.

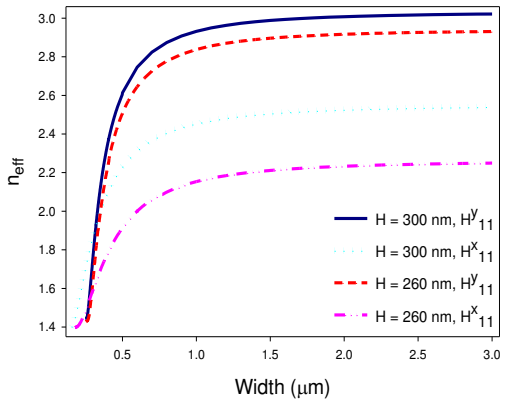

Fig. 2. Variations of the effective indices for the quasi-TE and quasi-TM modes with the waveguide width.

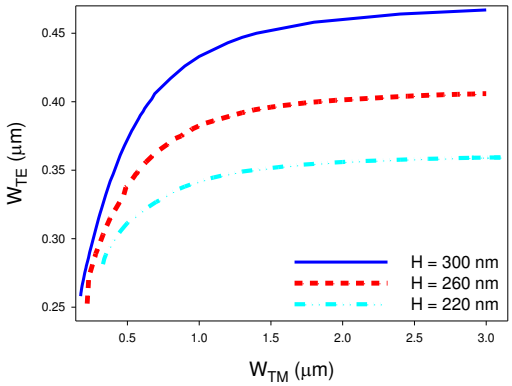

Fig. 3. The phase matching widths for quasi-TE and quasi-TM modes in two unequal waveguides.

Next, we considered a directional coupler, as shown in Fig.1 to obtain phase matching between the H^{y}_{11} and H^{x}_{11} modes of two waveguides. It is well known that for non-identical waveguides the loading of one waveguide to another are unequal for both of them. So, next the supermodes of this directional coupler structure are studied. In this case, width of one guide (W_{TE}) supporting quasi-TE mode is kept fixed at 353 nm, and width of the other waveguide (W_{TM}) is varied. Variation of the effective indices for the two supermodes are shown in Fig.4 for two different waveguide separations, *S*. It can be observed that for a larger separation, S = 200 nm, as the width, W_{TM} is

varied, effective index of one of the supermode remains almost constant. This supermode mostly looks like the H^{y}_{11} mode of guide 1 (quasi-TE mode in W_{TE} with a fixed width of 353 nm). On the other hand the effective index of the other supermode increases with the 2nd waveguide width, W_{TM} and this mode mostly resembles the H^{x}_{11} mode of this guide (W_{TM}). However, the effective index curves do not cross each other but like the supermodes of a directional coupler transform from one isolated mode to another. In this case, as we are phase matching the H^{x}_{11} mode of one guide (W_{TM}) with the H^{y}_{11} mode of another guide (W_{TE}), near the interactions region, two supermodes show the mixture of both the polarized modes which are highly hybrid in nature. For S = 200 nm, when W_{TM} = 577 nm, H^{x}_{11} mode of this guide is phase matched with the H^{y}_{11} mode of W_{TE} = 353 nm width. When the separation is reduced, the interactions between the polarized modes are more intense, which demonstrates a larger gap between the two effective indices near the phase matching. However, the phase matching width of 2nd guide, W_{TM}, changes as mutual loading of two unequal guides for different separations are also different.

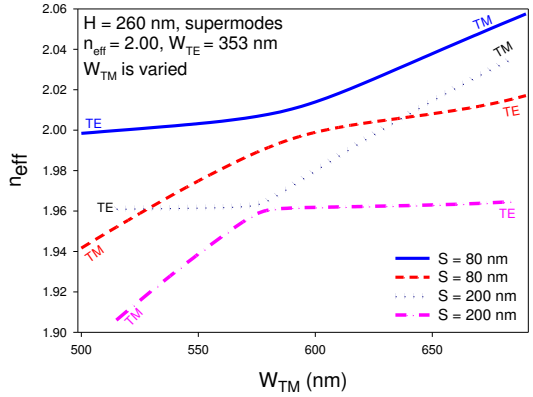

Fig. 4. Variation of the effective indices of two supermodes with the second guide width, W_{TM}.

Near the phase matching these supermodes are highly hybrid in nature and shows a combination of the both the polarized modes, and the field profiles of both the modes are shown next. The H_y Field profile of the upper branches of supermode is shown in Fig. 5 (a), when W_{TM} = 593 nm which illustrates the H_y field is mainly in the left waveguide (in W_{TE}). On the other hand, the H_x field profile of the same supermode shown in Fig. 5 (b) shows this component is predominantly in the right hand side guide, in W_{TM}. However, it can also be observed that field also spread in the other waveguide. In this case signs of both the H_x and H_y fields have nearly equal magnitudes and also have the same sign so the resulting polarization angle is 45 degrees with the x-axis.

Vector field profiles of the second supermode are shown in Fig. 6. Its H_x field is shown in Fig. 6 (a), which shows that it is mainly confined in right waveguide. On the other hand H_y field shown in Fig. 6 (b), shows that this field is mainly confined in the left waveguide. However, for this mode magnitude of the H_x and H_y fields were nearly equal but of opposite sign, so its resulting polarization angle is -4 opposite sign, so its resulting polarization angle is -45 degrees with the x-axis. It should be noted that the waveguide on the left (W_{TE}) had a fixed width and its quasi-TE mode was phase matched with the H^{x}_{11} mode of the right guide (W_{TM}), whose width was varied. Hence for both the supermodes, it can be observed that its H_x field was mainly in the left guide whereas H_y field was mainly in the right side waveguide.

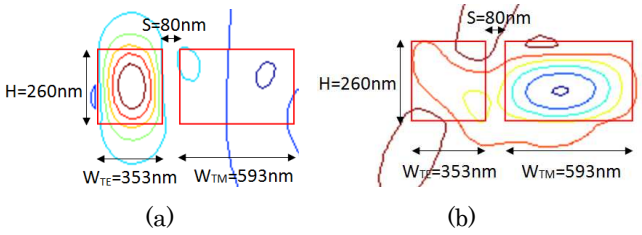

Fig. 5. (a) H_y field and (b) H_x field for the first supermode, W_{TM} = 593nm, W_{TE} = 353 nm, S= 80 nm.

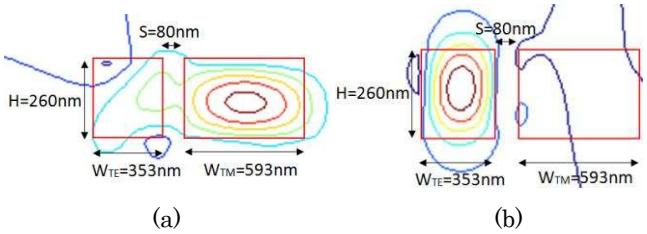

Fig. 6. (a) H_x field and (b) H_y field for the second supermode, when W_{TE} = 353 nm, W_{TM} = 593 nm, S= 80 nm.

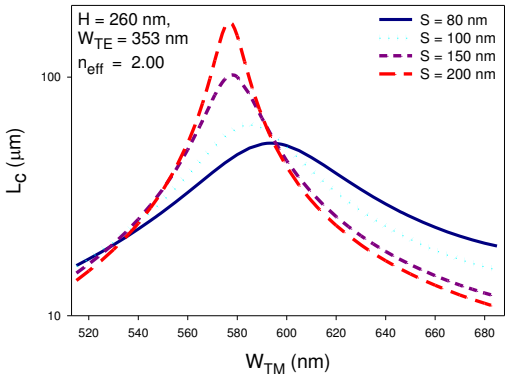

Fig. 7. Variations of the Coupling Length, L_c with the second waveguide width, W_{TM}, for different waveguide separations, S.

Variations of the coupling length with the second guide width (W_{TM}) are shown in Fig.7 for different waveguide separations. In this case width of the first NW (W_{TE}) was fixed at 353 nm supporting the quasi-TE mode. It can be noted that when phase matching was achieved the difference between the effective indices of the two supermodes were minimum and so the coupling length

shows a peak value. It can also be observed that coupling length is higher when separation is increased and its variation with the waveguide width (W_{TM}) is also sharper. It can be noted that phase matching width (W_{TM}) for separation S = 200 nm, 150 nm, 100 nm and 80 nm were respectively 577 nm, 578 nm, 585 nm and 593 nm, respectively (the width W_{TE} was kept constant at 353 nm). The changes in the phase matching condition are due to unequal loading on one guide by the other and this loading changes as the separation between the guides reduces. It should be noted that for smaller separation not only the coupling length is smaller, but it would be less sensitive with the change in the waveguide width.

The polarization rotator design presented here exploits two highly hybrid supermodes supported by a phase matched (between two different polarized modes) directional coupler. Variations of the modal hybridness of the first supermode with the waveguide width (W_{TM}) are shown in Fig. 8. It should be noted that when the two polarized modes in two waveguides are phase matched the magnitudes of the H_x and H_y fields are nearly equal (not exactly equal as their core areas were not identical) and hybridness increases. It can also be noted when separation between the waveguides is reduced, as shown by a solid dark blue line for S = 80 nm, the reduction of the modal hybridness is slower with the waveguide width variation allowing a more stabilized design.

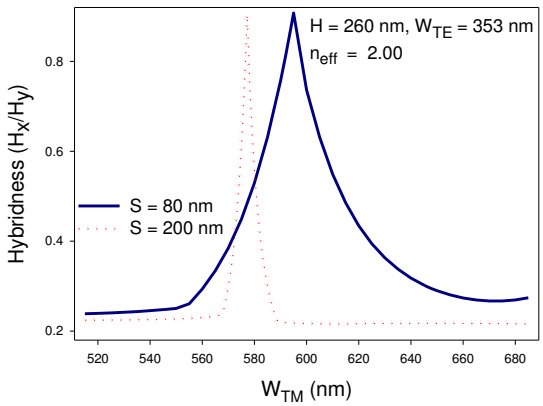

Fig. 8. Variations of the hybridness with the waveguide width, W_{TM} for the fundamental-TE (H^{y}_{11}) mode.

A quasi-TE mode in a standard silicon NW will have higher H_y field compared to its non-dominant H_x field. Now if this quasi-TE mode is launched at the start of the directional coupler section, this would excite two highly-hybrid supermodes, whose field profiles were shown in Figs. 5 and 6. The fundamental boundary conditions is the continuity of the tangential electric (E_t) and magnetic (H_t) fields at the dielectric interface. We have used the rigorous Least Squares Boundary Residual method [22] to implement these boundary conditions. This method yields the modal coefficients of the two supermodes excited in the directional coupler section. Variation of these two coefficients with the 2nd waveguide width are shown in Fig. 9, for two different separations, for S = 200 nm shown by two dashed lines and for S = 80 nm, shown by two solid lines. Here, in the horizontal axis instead of W_{TM}, we have used W_{TM}-W_{res}, to study the effect of fabrication tolerance, where W_{res} was the phase matching resonating width. It should be noted that for different waveguide separation, the phase matching width, W_{res}, were slightly different. When the W_{TM} is low and far away from the phase matching an incident H^{y}_{11} mode does not excite two polarized supermodes equally. In this case, the magnitude of the H^{y}_{11} mode (given by C_y) is nearly one and magnitude of the H^{x}_{11} mode (given by C_x) is nearly zero. However, when the waveguides are phase matched, these two supermodes are highly hybrid, then the magnitudes of the two polarized modes are nearly equal. Their values are nearly 0.707 = $\sqrt{2}$, indicating that each of the supermodes is carrying half power. By carefully observing the supermodes, it can be stated that a H^{y}_{11} mode in guide one, which has dominant H_y field in guide 1 will excite two supermodes (shown in Figs.5 and 6) and they must have similar magnitudes so that H_y field in guide 1 adds up but H_x fields in guide 2 will cancel to match the input H^{y}_{11} mode in the isolated input guide 1. It can also be noted that when separation is smaller, the variation of C_y and C_x are less sensitive with the waveguide change.

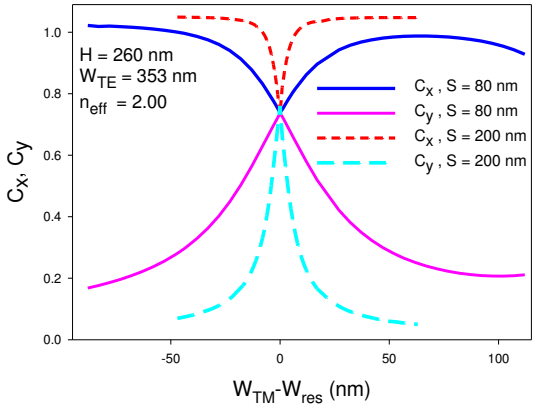

Fig. 9. The transmitted modal coefficient C_x, C_y with the width, W_{TM}-W_{res} for the waveguide.

Now, if the length of the directional coupler section is taken as L_c, then at this distance two excited supermodes would be out of phase and their vector addition will cancel the H_y field in guide 1 and add up the H_x field in guide 2 to yield a polarization rotated H^{x}_{11} mode in guide 2. From the modal coefficients shown in Fig. 9, and their full vectorial mode profiles polarized power in each waveguides can be calculated. Variations of the TM polarized power with H_x field in guide 2 and TE power with H_y field in guide 1 with the changes in waveguide width are shown in Fig. 10. In this case, instead its variation with the waveguide width, changes with the deviation from the idealised design are shown to study of the fabrication tolerances simultaneously. It can be observed that the maximum conversion for S = 200 nm and 80 nm, shown by cyan dash-

ed and dark blue dashed lines are about 0.985 and 0.99, respectively. The amount polarized power amount polarized power remains unconverted is shown as cross-talk (CT). It is shown here that for separation S =200 nm and 80 nm, shown by a red-dotted line and a dark pink dashed-dotted line, respectively, demonstrate that CT is better that – 18 dB for both the cases.

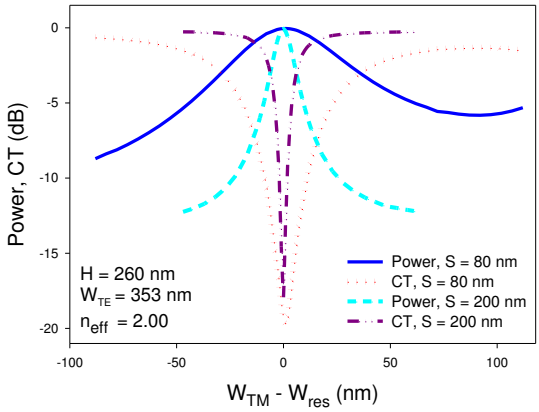

Fig.10. Variations of the polarization conversion and the polarization cross-talk with the width tolerance, W_{TM} - W_{res}.

The overall power loss is not shown here, but this value is less that 0.1 dB when the device is phase matched. It is shown here that for higher separation the performance is highly sensitive with changes in the waveguide dimension (here shown for width changes) but for a smaller separation this could be a viable design. It can be noted that when width is changed by 10 nm, due to fabrication error, the polarization conversion value deteriorates by only 0.6 dB, when S = 80 nm.

However, the curves above show the maximum polarization conversion and polarization cross-talk with the possible width variations, but still assumed to have the correct coupling length. But, in practice the fabrication errors cannot be anticipated so, the device length would be the same as originally designed when width deviation may appear. In this case as the coupling length will also change with the width variation, and next combined effect of these is also simulated.

Variations of the real polarization conversion for two different waveguide separations, S are shown in Fig.11. It can be observed the variation of polarization conversion is not monotonic as width is increased or reduced but shown with a periodicity. This is due to the effect of change in the coupling length. The length of the PR section is taken as the coupling length at the ideal design condition, L_{co} at the resonating case. But when width deviates from the design width, its coupling length reduces, which cannot be anticipated. When even multiple of this coupling length equals to the device length, all the polarized light reconverts to the original input polarization state, and overall polarization conversion will be zero, as shown here. The zero conversions are related to the case when the modified coupling length (due to fabrication error) is $2m$ times smaller than the originally designed length consider for this polarization rotator when m is an integer. It can be observed that, for with S = 200 nm as shown by red dashed curves, even a small change of 10 nm in the width the resulting polarization conversion can drop to zero, and this would be very difficult to control.

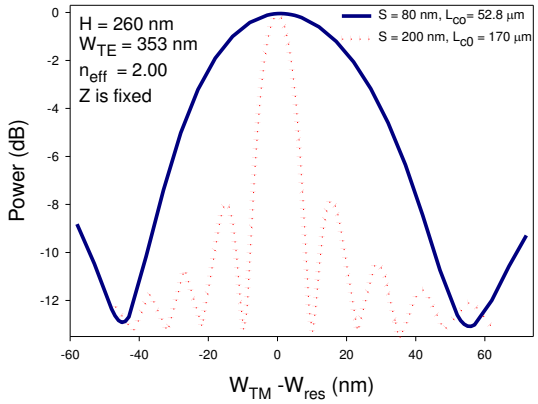

Fig. 11. Variations of the converted power P_x at Z = 52.8 μm an Z = 170.0 μm, with the waveguide width W_{TM}-W_{res}.

On the other hand, for S = 80 nm, shown by a solid blue line, polarization rotation drops to zero only when ΔW is 45 nm, as in this case coupling length becomes half. However, for ΔW = 10 nm, the polarization rotation will be 85 %, which could still be acceptable as a practically achievable and a viable design. Effect of fabrication tolerances for the other waveguide, W_{TE}, or separation between the waveguides are also similar but not shown here.

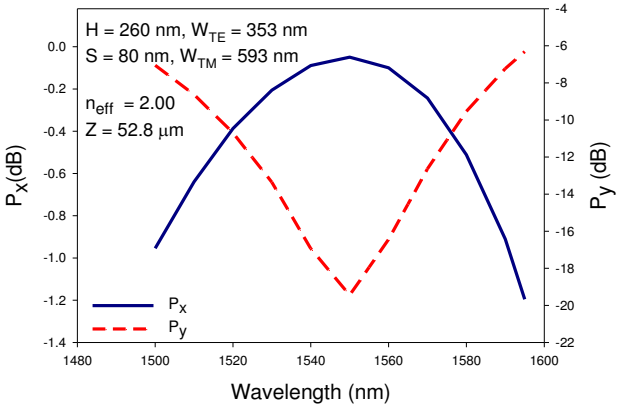

Fig. 12. Variation of the polarization conversion and polarization cross-talk with the operating wavelength.

Finally, the effect of operating wavelength variation on the performance of this PR is studied. Although, as the wavelength changes, coupling length also changes and this will also change the phase matching conditions, however, in this design, as the waveguide separation was very small, coupling was strong, the effect of small change in the wavelength is almost negligible, as shown here.

This suggests the devices will have a large operating bandwidth.

The effect of temperature variation has also been studied at but this is not shown here. It was identified that a small amount of temperature tuning can be possible, which can be used to compensate fabrication tolerances, but this tuning range is rather very small. Similarly, the previous figure indicates a small amount of wavelength tuning can also be used to compensate the fabrication tolerances.

4. Conclusions

The design presented here uses two simple silicon nanowires, which would be simpler than the design approaches reported earlier by using slot waveguides [12-15]. As this structure does not consider any bend section or slanted side wall [8-10] or trench with different etching depth [11], it would be simpler to fabricate using a single mask.

Through a detailed numerical study, a novel design of a compact SOI polarization rotator incorporating polarized coupling between two unequal wide waveguides is reported here. The above results suggests that an appreciable short 52.8 μm long PR can be designed for 1.55 μm wavelength by exploiting the phase matching between the orthogonally polarized modes of these two guides. Maximum power coupling efficiency of 99% is possible from input TE (or TM) to output TM (or TE) mode, with cross-talk better than -20 dB and loss value lower than 0.1 dB. Fabrication tolerances of the designed structure were studied by varying different WG parameters and we have suggested that, a part of it may be corrected through appropriate temperature tuning or by wavelength adjustment.

Thus, this high conversion efficiency, low footprint, simpler design, along with the existence of well-matured fabrication technologies for SOI structures, should make our proposal attractive for making an on-chip polarization rotator for their potential deployment. This design should be relatively easy to implement for fabrication and can be made with a single mask. It is also shown here that operating bandwidth of these PR is considerable wider and suitable for WDM applications.

References

1. M. Lipson, "Guiding, modulating, and emitting light on silicon-challenges and opportunities," J. Lightwave Technol. **23**, 4222-4238 (2005).
2. R. C. Alferness and L. L. Buhl," High-speed waveguide electro-optic polarization modulator," Opt. Lett. 500–502 (1982).
3. M. Schlak, C. M. Weinert, P. Albrecht, and H. P. Nolting, Tunable TE/TM-mode converter on (001)-InP-substrate, IEEE Photon. Technol. Lett. **3**, 15–16 (1991).
4. K. Mertens, B. Scholl, and H. J. Schmitt," Strong polarization conversion in periodically loaded strip waveguides," IEEE Photon. Technol. Lett. **10**, 1133–1135 (1998).
5. Y. Shani, R. Alferness, T. Koch, U. Koren, B. I. Miller, and M. G. Young," Polarization rotation in asymmetric periodic loaded rib waveguides," Appl. Phys. Lett. **59**, 1278-1280 (1991).
6. S. S. A. Obayya, B. M. A. Rahman, K. T. V. Grattan and H. A. El-Mikati," Analysis of polarization rotation in cascaded optical waveguide bends," IEE Proc.-Optoelectron. **149**, 75-80 (2002).
7. B. E. Little and S. T. Chu," Theory of polarization rotation and conversion in vertically coupled microresonators," IEEE Photon. Technol. Lett. **12**, 401–403 (2000).
8. H. Deng, D. O. Yevick, C. Brooks, and P. E. Jessop, "Design rules for slanted-angle polarization rotators," J. Lightwave Technol. **23,** 432–445 (2005).
9. B. M. A. Rahman, S. S. A. Obayya, N. Somasiri, M. Rajarajan, K. T. V. Grattan, and H. A. El-Mikathi,," Design and characterization of compact single-section passive polarization rotator," J. Lightwave Technol. **19**, 512–519 (2001).
10. C. Brooks, P. E. Jessop, H. Deng, D. O. Yevick, and G. Tarr, "Passive silicon-on-insulator polarization-rotating waveguides, " Opt. Eng. **45**, 044603 (2006).
11. D. M. H. Leung, B. M. A. Rahman, and K. T. V. Grattan, "Numerical analysis of asymmetric silicon nanowire waveguide as compact polarization rotator," IEEE Photon. J. **3** 381-389 (2011).
12. N. N. Feng, R. Sun, J. Michel, and L. C. Kimerling, "Low-loss compact-size slotted waveguide polarization rotator and transformer," Opt. Lett. **32**, 2131-2133 (2007).
13. B. Wohlfeil, L. Zimmermann, and K. Petermann, "Asymmetric codirectional coupler between regular nanowaveguide and slot-waveguide for polarization conversion," OSA Adv. Photon. Congress, **ITu2B5** (2012).
14. Y. Fei, L. Zhang, T. Cao, Y. Cao, and S. Chen, "Ultracompact polarization splitter-rotator based on asymmetric directional coupler," Appl. Opt. **51**, 8257-8261 (2012).
15. A. Bahr, B. M. A. Rahman, R. K. Varshney, and B. P. Pal, "Design and performance study of a compact SOI polarization rotator at 1.55 μm," J. Lightwave Technol. **31**. 3687-3693 (2013).
16. M. Komatsu, K. Saitoh, and M. Koshiba, "Design of miniaturized silicon wire and slot waveguide polarization splitter based on a resonant tunneling." Opt. Express **17**, 19225-19234 (2009).
17. X. Zhi-Gang, L. Zhi-Yuan, and Z. Dao-Zhong, " TM-like and TE-like modes coupling in a two dimensional photonic crystal slab composed of truncated cone silicon rods," Chin. Phys. Lett. **25** 2089-2092 (2008).
18. T. Baba "Si photonic wire waveguides" Proc. SPIE , **5515**, 150-157 (2004).
19. S. A. A. Obayya, B. M. A. Rahman, K. T. V. Grattan, and H. A. El-Mikati, " Improved design of a polarization converter based on semiconductor optical waveguides bends," Applied Optics, **40**, 5395-5401 (2001).
20. B. M. A. Rahman and J. B. Davies, " Finite element solution of integrated optical waveguides," J. Lightwave Technol. **2**, 682–688 (1984).
21. S. S. A. Obayya, B. M. A. Rahman, and H. A. El-Mikati, "New full-vectorial numerically efficient propagation algorithm based on the finite element method," J. Lightwave. Technol **18**, 409–415 (2000).
22. B. M. A. Rahman and J. B. Davies, "Analysis of optical waveguide discontinuities," J. Lightwave Technol **6**, 52–57 (1988).